Macromolecular Bioscience
www.mbs-journal.de

One-Step Labeling of Collagen Hydrogels with Polydopamine and Manganese Porphyrin for Non-Invasive Scaffold Tracking on Magnetic Resonance Imaging

*Daniel Andrzej Szulc and Hai-Ling Margaret Cheng**

Biomaterial scaffolds are the cornerstone to supporting 3D tissue growth. Optimized scaffold design is critical to successful regeneration, and this optimization requires accurate knowledge of the scaffold's interaction with living tissue in the dynamic in vivo milieu. Unfortunately, non-invasive methods that can probe scaffolds in the intact living subject are largely underexplored, with imaging-based assessment relying on either imaging cells seeded on the scaffold or imaging scaffolds that have been chemically altered. In this work, the authors develop a broadly applicable magnetic resonance imaging (MRI) method to image scaffolds *directly*. A positive-contrast "bright" manganese porphyrin (MnP) agent for labeling scaffolds is used to achieve high sensitivity and specificity, and polydopamine, a biologically derived universal adhesive, is employed for adhering the MnP. The technique was optimized in vitro on a prototypic collagen gel, and in vivo assessment was performed in rats. The results demonstrate superior in vivo scaffold visualization and the potential for quantitative tracking of degradation over time. Designed with ease of synthesis in mind and general applicability for the continuing expansion of available biomaterials, the proposed method will allow tissue engineers to assess and fine-tune the in vivo behavior of their scaffolds for optimal regeneration.

1. Introduction

Scaffolds are an essential ingredient in many tissue engineering strategies. Whether they are synthetic or derived from natural materials, scaffolds help support tissue formation in three dimensions and are pivotal to growing thick tissue. They allow cells to penetrate, attach, and migrate; they retain biochemical factors conducive to tissue growth; and they biodegrade over time at a rate ideally matched to that of new extracellular matrix production as new tissue forms. One of the major challenges facing scaffold development, however, is proper optimization for desired in vivo function. Accurate characterization of in vivo behavior and especially kinetics cannot be predicated on in vitro degradation studies, since the transition from an in vitro to an in vivo setting often results in vast changes in a material's structure, properties, and function. Thus, accurate in vivo imaging techniques for scaffold monitoring are crucial for optimizing tissue-engineered scaffolds in the intended biological environment. However, imaging applications to date have focused largely on implants with an innate, stark contrast difference relative to native tissue. For natural scaffolds that are more difficult to distinguish due to similar contrast levels, scaffold monitoring has been tackled indirectly. For example, one method has been to image the cells that are seeded onto a scaffold,[1,2] but this approach provides no information on the evolving scaffold structure and is inappropriate for acellular matrix-based regeneration methods. The ability to image the implanted scaffold *directly* in vivo remains largely unexplored, but would yield critical information on degradation, host-tissue interactions, and restoration of tissue function.

Non-invasive imaging technologies such as magnetic resonance imaging (MRI) hold significant potential for scaffold monitoring in tissue engineering. MRI provides fine spatial resolution, deep tissue penetration, and superior soft-tissue contrast. To enable direct monitoring of scaffolds in vivo, we adopt a different approach using MRI. We do not image labeled cells in the scaffold or rely on intrinsic contrast differences from native tissue arising from biochemical and structural differences. Instead, we directly label the scaffold with a "bright" MRI contrast agent to provide scaffold identification regardless of its biochemical makeup. Unlike the handful of existing reports that attempt to track scaffolds directly using iron oxide-based "dark" imaging,[3–5] we adopt a positive-contrast "bright" method. Positive-contrast imaging offers the benefit of greater specificity in where the signal comes from and the potential to quantify contrast agent concentration, and therefore scaffold content, in absolute terms. This potential for quantification is a must if we need to monitor degradation in meaningful units.

D. A. Szulc, Prof. H.-L. M. Cheng
Institute of Biomaterials & Biomedical Engineering
The Edward S. Rogers Sr. Department of Electrical & Computer Engineering
Ted Rogers Centre for Heart Research
Translational Biology & Engineering Program
University of Toronto
164 College Street, RS407, Toronto, ON M5S 3G9, Canada
E-mail: hailing.cheng@utoronto.ca

The ORCID identification number(s) for the author(s) of this article can be found under https://doi.org/10.1002/mabi.201800330.

DOI: 10.1002/mabi.201800330

To achieve strong "bright" scaffold imaging, we utilize manganese (Mn), an endogenous MRI-active metal that is significantly less toxic than gadolinium (Gd) in free ionic form. The Mn ion is coordinated in a porphyrin ring to produce a manganese porphyrin (MnP) structure that yields excellent contrast enhancement.[6] The porphyrin ring binds the Mn ion with high thermodynamic and kinetic stability, thus conferring safety. Importantly, the ring also allows facile chemical functionalization[6] to enable labeling a wide variety of scaffold materials. To create a flexible labeling strategy, we sought to develop a simple labeling method that did not rely on the chemical make-up of the scaffold. For this, we turned to polydopamine (PDA), a bio-inspired polymer that has been found to coat various surfaces ranging vastly in material properties and composition.[7] The versatility, facile synthesis, and biocompatibility of PDA made it an ideal candidate for use in a universal labeling method.[8] We report here the first approach using MRI and positive-contrast MnP to directly label scaffolds via a universal adhesive for non-invasive scaffold monitoring.

2. Results and Discussion

The feasibility of in vivo scaffold monitoring depends a great deal on the sensitivity provided by the contrast agent used for labeling. In our approach, we use Mn for positive contrast enhancement, as it provides a key advantage over Gd-chelates traditionally used for bright imaging: lower toxicity. Manganese is a vital mineral naturally found in the human body and plays a role in many intracellular activities such as bone mineralization, enzyme activation, metabolism, and cellular protection from free radical species.[9] Manganese amounts in the body range from 10 to 20 mg distributed amongst many tissues with primary accumulation in the blood and liver.[9] Epidemiological studies have shown that doses as high as 11–15 mg per day cause no adverse effects in adult humans, with excess Mn being excreted via feces and trace amounts via urine.[9–11] In our study, very low doses of Mn (5.49×10^{-3} to 2.196×10^{-2} mg per scaffold) were required to achieve significant MRI signal and, thus, posed no safety threat. Furthermore, blood-pool Mn can be shuttled around the body by transferrin, and at the cellular level Mn enters cells via assisted passive transport by specific transporters such as the divalent metal transporter-1 to act as a co-factor for many different enzymes and metabolic processes.[9] In contrast, Gd is not an endogenous metal and its accumulation has been linked to toxicity in both immediate and long term exposures in human patients.[6,12–14] While many Gd-based contrast agents (GBCA) are still clinically used, the recent bioaccumulation and toxicity findings have led to legal bans and the removal of some GBCA's from the market while others have been restricted in their clinical use.[12] In addition to its enhanced safety novel, Mn chelates have been designed so that they exhibit a greater number of water binding sites, resulting in greater contrast enhancement than traditional Gd-chelates.[6] Collectively, these attributes have made Mn-based compounds a very promising new class of positive-contrast MRI agents. Within the class of Mn agents exists a subclass known as MnPs, which consist of a Mn core chelated by a porphyrin ring. An MnP contrast agent, $MnPNH_2$, was designed and synthesized in this study as per the reaction scheme shown in **Figure 1**A. The structure and purity of the intermediates and final product was determined by ultraviolet (UV)-visible spectra, ^1H nuclear magnetic resonance (NMR), high perform liquid chromatography (HPLC), flame atomic absorption spectroscopy (FAAS), and mass spectroscopy (Figures S1–S4, Supporting Information).

The porphyrin ring of the contrast agent not only chelates the Mn metal, inhibiting demetallation in the body, but also allows for facile chemical modification and, thus, control of its chemical reactivity. To create a contrast agent ideal for scaffold labeling in vivo, the porphyrin ring was modified to enhance its excretion and its ability to be chemically linked to other compounds for labeling and tracking purposes. To meet these requirements, the porphyrin ring was functionalized with a single nucleophilic amine group and three highly hydrophilic sulfate groups. The single amine group acts as a chemical point of attachment. Amine functionalized molecules are used extensively in biological conjugation reactions, because they contain an active lone pair of electrons on the electronegative nitrogen atom. This makes amines very nucleophilic and easily conjugated to a variety of other chemical groups.[15] The three sulfate groups increase the porphyrin's water solubility, which is essential for the agent to be transported via the circulatory system.[6,16,17] In summary, the structure of the $MnPNH_2$ contrast agent was designed to facilitate both easy conjugation to a scaffold's molecular backbone and excretion from the body after the scaffold degrades.

In addition to providing sensitive detection, safety, and biocompatibility, the scaffold labeling approach must also be simple and applicable to a wide variety of materials. To meet these requirements, we utilized a bio-inspired adhesive polymer, PDA, to adhere the MRI contrast agent to a scaffold. Polydopamine is easily formed by the self-polymerization of dopamine in slightly basic physiological solutions. It deposits and adheres to a variety of biomaterials and demonstrates favorable biocompatibility.[18] Another relevant feature is the strong conjugation of PDA coatings with amine-functionalized compounds, whereby the amine compound covalently attaches to the PDA monomers via a Schiff base reaction or a Michael-type addition (Figure 1B).[19] These properties favor PDA as an ideal platform for adhering $MnPNH_2$ to a variety of scaffold materials for in vivo tracking.

As proof-of-principle, collagen hydrogel, a biomaterial that is highly tunable and used extensively in tissue engineering, was used as a prototype scaffold.[20–26] Collagen hydrogels have a molecular structure that promotes cell attachment and growth, and its physical properties can be easily modified with a variety of cross-linking agents. To determine the most ideal method of scaffold labeling, three facile, efficient, and versatile protocols were tested for passive and active incorporation of $MnPNH_2$ into collagen scaffolds (**Figure 2**). Two of these protocols use dopamine, which is known to polymerize in the presence of collagen while maintaining its adhesive character.[27–29]

Method 1 passively entraps $MnPNH_2$ into the collagen scaffold prior to thermal cross-linking and gelation. Method 2 actively incorporates $MnPNH_2$ into the scaffold by conjugation to a PDA-collagen gel, analogous to similar methods for the formation of collagen-PDA scaffolds and collagen-PDA scaffold functionalization.[28,30] Method 3 actively incorporates

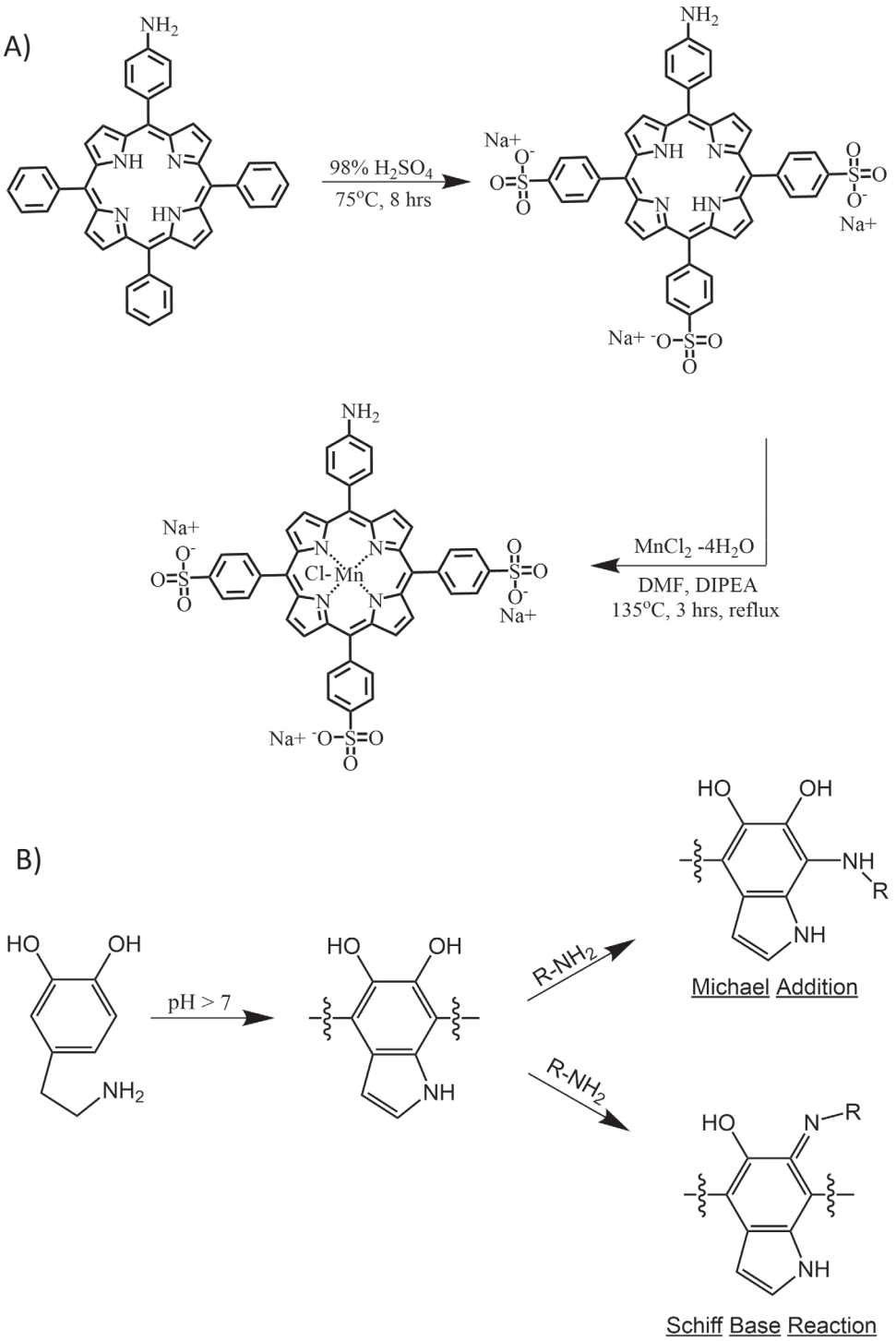

Figure 1. Reaction scheme illustrating the synthesis of MnPNH2, PDA and PDA's secondary functionalization routes. A) $MnPNH_2$ was synthesized from a porphyrin precursor. The precursor was then functionalized with peripheral sulfates groups and subsequently a primary amine group. B) Dopamine self-polymerizes at slightly basic conditions resulting in PDA, which can be functionalized with amine-containing compounds via Schiff base reaction and Michael-type additions.

$MnPNH_2$ into the scaffold by the simultaneous reaction of dopamine and $MnPNH_2$ in one pot with collagen. Method 1 was developed to determine if $MnPNH_2$ would itself bind non-covalently to the scaffold. Methods 2 and 3 examined the need for a temporal separation between collagen-PDA formation and $MnPNH_2$ conjugation. This was done to determine the simplest yet most efficient method of labeling the scaffold. After labeling, gelation, and sufficient washing, the gels were

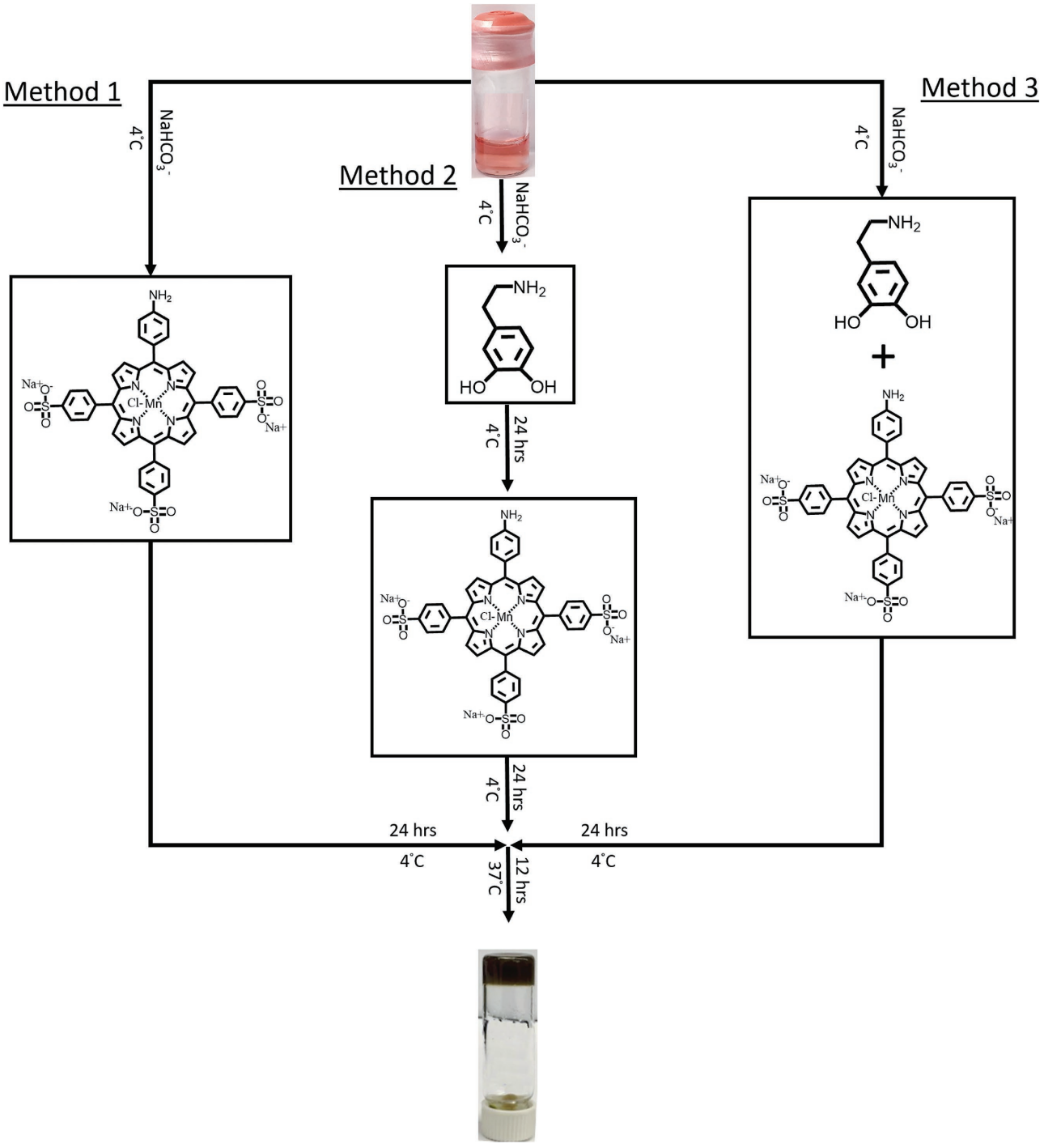

Figure 2. Collagen hydrogel labeling reaction scheme. Three different methods were tested. Method 1 involved passively incorporating $MnPNH_2$ into a neutralized (pH 7.4) collagen solution prior to thermal cross-linking/gelation. Method 2 involved mixing collagen with dopamine and then $MnPNH_2$ prior to gel formation. Method 3 involved mixing collagen with dopamine and $MnPNH_2$ in one pot prior to gel formation.

imaged on a clinical 3-Tesla MRI scanner. T_1- and T_2-weighted images were acquired (**Figure 3**A,B), and quantitative T_1 and T_2 relaxometry maps were measured (Figure 3C,D). A reduction in T_1 and T_2 relaxation times for labeled scaffolds relative to unlabeled scaffolds could be detected in all three methods and $MnPNH_2$ concentrations tested, as expected for a T_1 agent. A maximum T_1 reduction of sixfold relative to control and a maximum T_2 reduction of fourfold were achieved for the conditions tested (Figure 3E,F). This is consistent with literature,[31] where MnP derivatives act primarily as positive-contrast T_1 agents but also exert dual activity as moderate T_2 agents. Comparison amongst all three labeling protocols demonstrated that

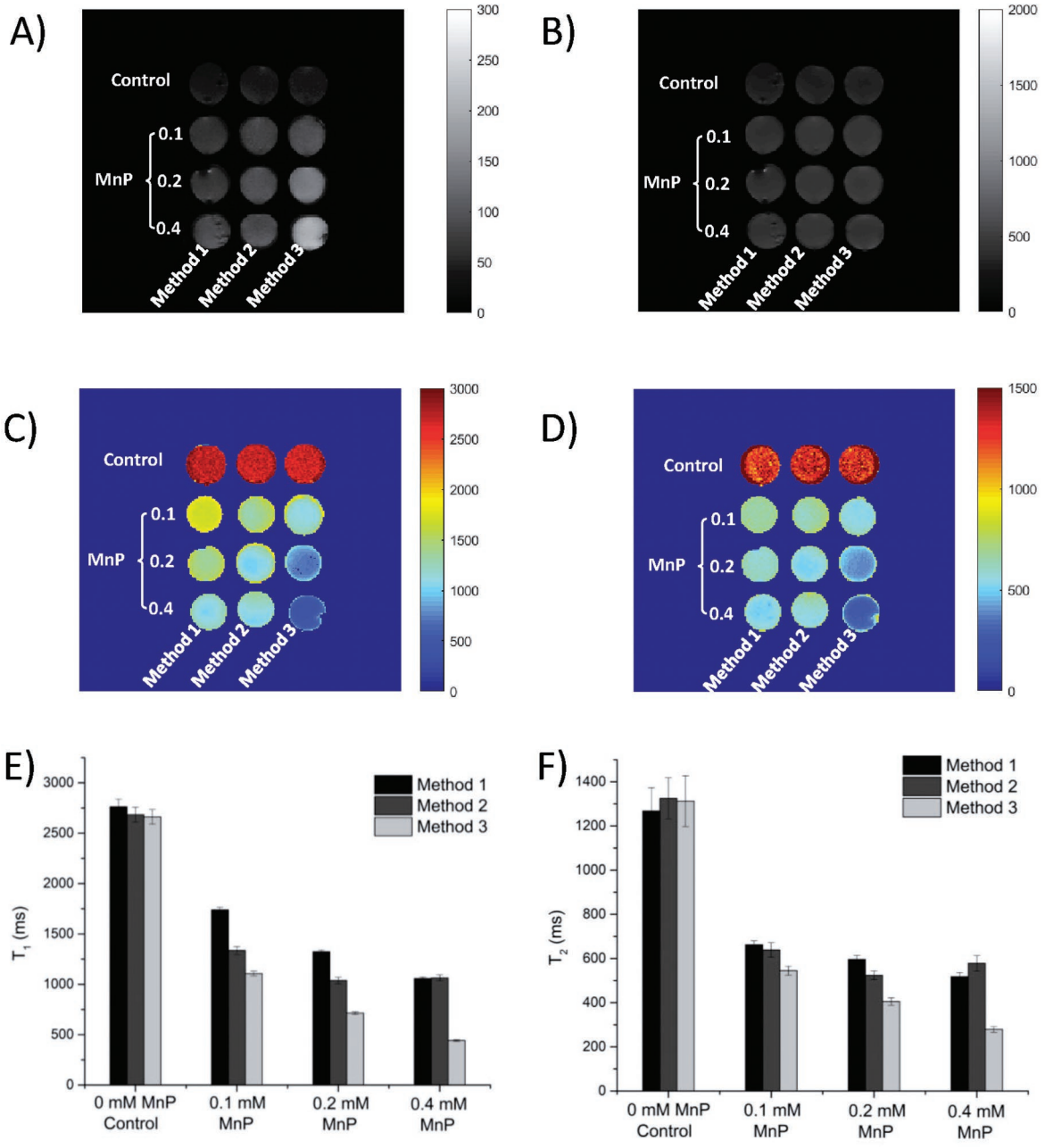

Figure 3. Comparison of methods for labeling collagen hydrogel scaffolds on MRI. Scaffolds labeled using different methods and concentrations of $MnPNH_2$ (0, 0.1, 0.2, and 0.4 mM) are shown on a A) T_1-weighted image, B) T_2-weighted image, C) map of T_1 relaxation times, and D) map of T_2 relaxation times. Methods 2 and 3 incorporated 0.25 mM of dopamine-hydrochloride. E,F) Graphs of T_1 and T_2 relaxation times show a significant difference in T_1 and T_2 across different $MnPNH_2$ concentrations ($p < 0.05$). However, while T_1 was significantly different amongst all methods, T_2 was different only for Method 3 ($p < 0.05$). Shown are mean values and standard deviations.

Method 3 exhibited the largest reductions in T_1 times at all $MnPNH_2$ concentrations and, thus, the greatest positive signal (Figure 3A,E). Furthermore, the uniformity of the bright signal throughout the gel (Figure 3A) indicates uniform dispersion and attachment of the contrast agent. There are multiple potential reasons for the enhanced reductions achieved by Method 3; however, we hypothesize that it is simply due to the availability of coupling sites between PDA and $MnPNH_2$. As dopamine reacts and becomes PDA, it will interact with any free amines (present both on collagen and on $MnPNH_2$). Thus, in Method 2, since PDA is formed in the presence of collagen first, it can bind many coupling sites, leaving fewer available for binding to $MnPNH_2$. This results in higher T_1 values and also binding saturation, which is seen at higher $MnPNH_2$ loading concentrations for Method 2. However, in Method 3, $MnPNH_2$ is present as the PDA forms; thus, there is more competition for binding

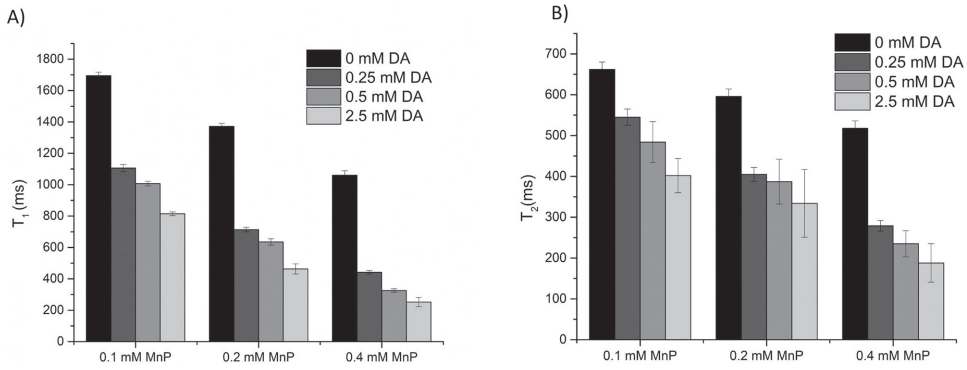

Figure 4. Effect of dopamine (DA) and $MnPNH_2$ concentration on labeling. A) T_1 and B) T_2 relaxation times of collagen hydrogels labeled with $MnPNH_2$ using Method 3 demonstrate the T_1- and T_2-reducing effects of increasing concentrations of either $MnPNH_2$ or the adhesive. Samples were extensively washed before imaging. Significant differences in T_1 and T_2 exist across different DA and $MnPNH_2$ concentrations ($p < 0.05$). Shown are mean values and standard deviations.

sites and more $MnPNH_2$ can bind, which is evident by the enhanced contrast and larger reductions in T_1 at all labeling concentrations. These results provide solid proof-of-principle evidence for the ability to label and visualize collagen gels by MRI, with the highest signal and lowest T_1 times produced by the one-pot labeling approach (Method 3). It is worth noting that the passive approach (Method 1) resulted in significant contrast enhancement also; however, this enhancement may not be sufficient for visualizing a scaffold as it degrades in the body and further lowers signal contrast.

Upon identifying Method 3 as the most effective for scaffold labeling, an additional range of dopamine concentrations (0–2.5 mM) and $MnPNH_2$ concentrations (0.1–0.4 mM) were tested to determine the optimal ratio of $MnPNH_2$:PDA for labeling. Labeled scaffolds were scanned on MRI as before. A reduced T_1 and T_2 was observed with either increasing $MnPNH_2$ concentrations or increasing PDA concentrations, or both, with a 1.53 to 4.2-fold T_1 reduction and 1.2 to 2.76-fold T_2 reduction from passively labeled (no PDA) to actively labeled scaffolds (with PDA) (**Figure 4**). It is important to note that a large reduction in T_1 versus control was observed even with the lowest concentration of $MnPNH_2$ and PDA, thus demonstrating the capability of Method 3 to produce large contrast enhancement with very small amounts of labeling agents. This data provides a useful scale for determining the ideal $MnPNH_2$:PDA ratio required to achieve optimal contrast on MRI in any specific in vivo setting. However, since the T_1 of the labeled scaffold (250–750 ms) is considerably lower than the range of T_1s of different organs (brain gray matter $T_1 = 1615 \pm 149$ ms, skeletal muscle $T_1 = 1509 \pm 150$ ms, myocardium $T_1 = 1341 \pm 32$ ms at 3.0 Tesla[32]), it is relatively straightforward to achieve extremely high contrast for the labeled scaffold in vivo in nearly all tissues in the body.

Initial proof-of-principle studies for monitoring scaffold degradation was conducted by degrading labeled and unlabeled gels enzymatically with collagenase in vitro (**Figure 5**). Gels were prepared and degraded with different concentrations of collagenase for the same amount of time (4 h) to prevent differences arising from hydrolytic degradation. Degradation was assessed by MRI of the gel and UV absorbance of the degraded solution (Figure 5A–F). The characteristic absorbance profile of $MnPNH_2$ was only observed in degraded solutions containing $MnPNH_2$-conjugated gels (Figure S5, Supporting Information), and the absorbance intensity at λ_{max} (468 nm) correlated positively with gels loaded with more collagenase, indicating greater degradation as expected (Figure 5E). UV absorbance intensities were also highly consistent within a sample group, and between groups, exhibiting a stable and controlled release profile rather than a burst model, indicative of strong binding to the collagen gel. The degradation trend was further confirmed by volumetric MRI, which provided an accurate volumetric analysis of labeled gels and indicated significant surface degradation, with a negative correlation between gel size and collagenase loading (Figure 5F). Potential bulk degradation throughout the scaffold was assessed on quantitative T_1 and T_2 maps. The interiors of scaffolds were minimally degraded, as judged by a relatively constant signal between sample groups on MRI; however, the small increase in T_1 and T_2 and the corresponding decrease in signal-to-noise ratios was statistically significant, indicating the possibility to detect with MRI slight changes in density in labeled scaffolds (Figure 5D). This is possible as the signal measured by MRI is directly proportional to contrast agent concentration. Since in our case the contrast agent is adhered to the collagen fibers, the local concentration now reflects the density of the scaffold/fibers. This observation was confirmed qualitatively on scanning electron microscopy (SEM) by porosity and fiber density of the degraded scaffolds. After MRI, the scaffolds were flash frozen and lyophilized to maintain their structure. They were then imaged by an environmental SEM to visualize changes in pore size. SEM images in Figure 5G show that all scaffolds maintained a similar pore size and fiber density, corroborating the finding of minimal bulk degradation. The sensitivity of MRI to microstructural alterations was further validated with a collagen contraction model. In this model, it was expected that as the collagen fibers contracted, the conjugated $MnPNH_2$ molecules would move with them; thus, as the density of collagen increased, so would the local concentration of $MnPNH_2$, creating a spatially isolated area of high concentration and high signal. As seen in Figure 5H, the contracted gel exhibited a much higher signal indicative of a higher $MnPNH_2$

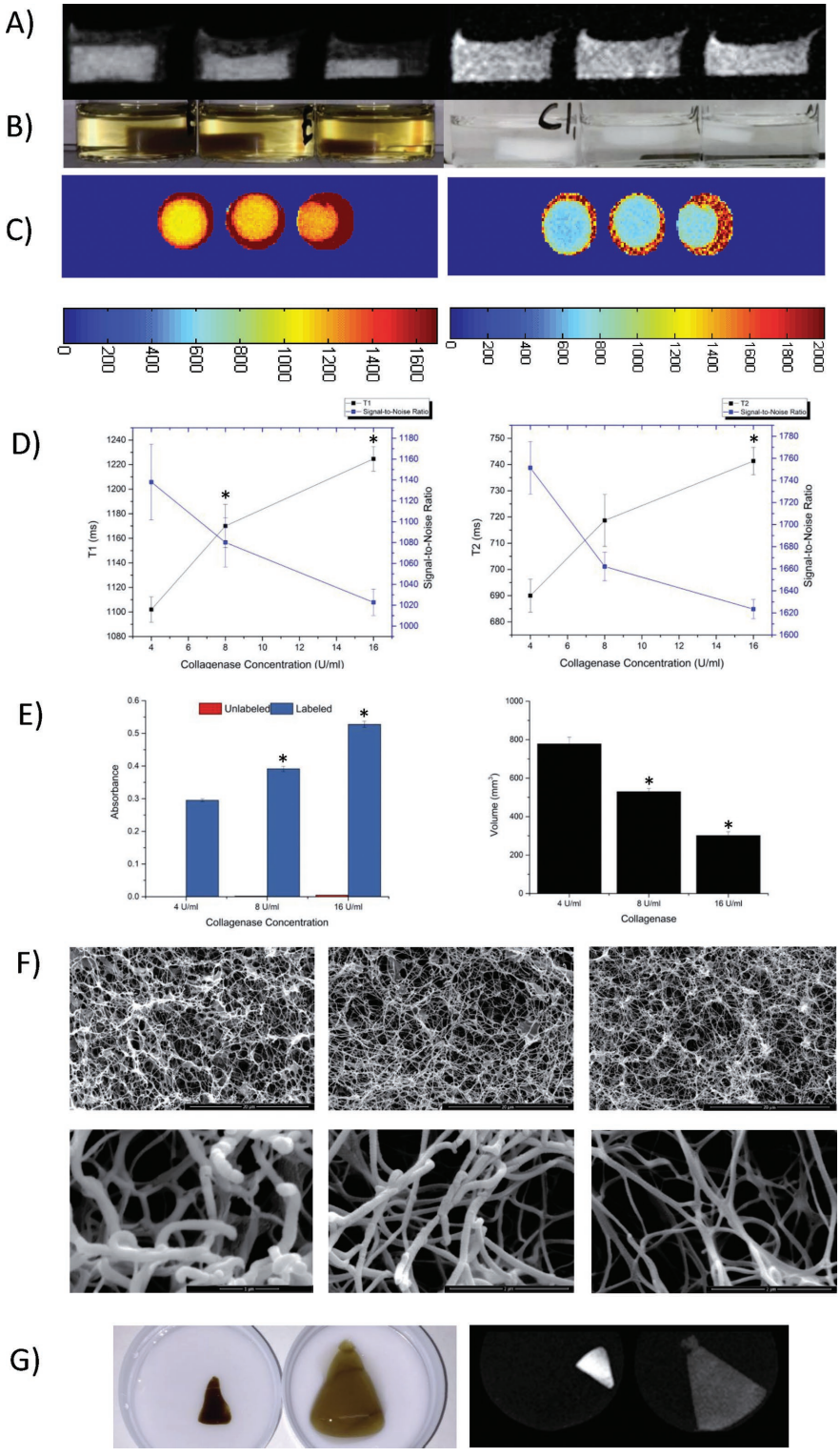

Figure 5. Monitoring in vitro degradation with MRI. Collagen gels degraded enzymatically for a fixed time interval with varying amounts of collagenase (4, 8, and 16 U mL^{-1}) were assessed on MRI and UV. A) T_1-weighted MR images of labeled (left) and unlabeled (right) collagen gels degraded with 16, 8, and 4 U mL^{-1} collagenase from left to right. B) Corresponding photographs of degraded gels. C) Maps of T_1 and T_2 relaxation times (ms) of the labeled gels and D) corresponding mean values and signal-to-noise ratios (SNR). E) UV analysis of the degraded gel solution with peak absorbance at 468 nm (left) and MRI volumetric analysis of the labeled gels (right). F) SEM of degraded gels with 4, 8, and 16 U mL^{-1} of collagenase from left to right. G) Photographs of contracted and non-contracted gels (left) and the corresponding T_1-weighted image on MRI (right). *Denotes significant differences ($p < 0.05$).

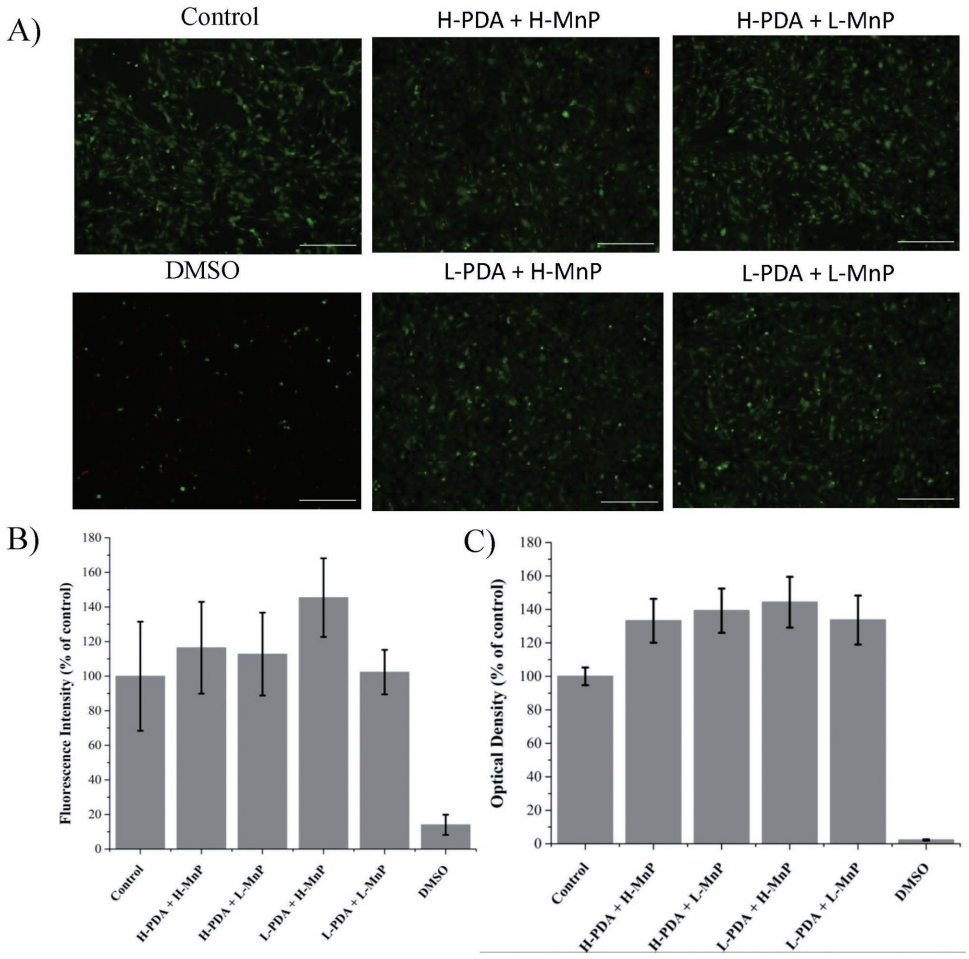

Figure 6. Biocompatibility of labeled scaffolds. HUVEC cells were seeded and cultured on collagen gels for 48 h before A) live (green) and dead (red) staining, scale bar 400 um, B) live cell DNA proliferation assay, and C) WST-1 metabolic activity assay. H-PDA and L-PDA represent high (2.5 mM) and low (0.25 mM) dopamine labeling, while H-MnP and L-MnP represents high (0.4 mM) and low (0.1 mM) MnP-NH2 labeling. DMSO controls were treated with 5% DMSO.

concentration. Further validation is required to assess the capability of this technique to accurately measure scaffold changes in fiber density; however, this result serves as a testament to the sensitivity of MRI for non-invasive scaffold monitoring.

To evaluate the biocompatibility of the labeled collagen gels, a series of scaffolds were assessed for their ability to promote cell attachment and growth. Scaffolds were prepared with various ratios of dopamine and $MnPNH_2$ as before and seeded with primary human umbilical vein endothelial cells (HUVEC). The cells were grown for 48 h and then assayed for metabolic activity, live cell DNA content, and live/dead staining (**Figure 6**). HUVEC cells were chosen as a prototypical cell type for their application in tissue engineering and regenerative medicine, where they have been utilized extensively with collagen scaffolds to promote endothelialization and angiogenesis.[33,34] Scaffolds prepared with both high and low amounts of dopamine and $MnPNH_2$ exhibited statistically similar levels of live cell DNA content and metabolic activity compared to control collagen scaffolds (Figure 6B,C). This demonstrated that both labeled and unlabeled scaffolds promoted similar rates of cellular proliferation and metabolism. Furthermore, live/dead staining of the cells under all conditions, except for the dimethyl sulfoxide (DMSO) negative control, showed very low to no dead cells (Figure 6A), further supporting the biocompatibility and nontoxic properties of the labeled scaffolds. Additionally, on all scaffolds a flatten and spread cell morphology as opposed to a rounded shape was found. This is distinctive for healthy proliferating cells and indicative of the ability of the scaffolds to promote cell adhesion. Despite the absence of statistical differences, it is worth noting the slightly elevated averages in metabolic activity and DNA cell content, which correlates well with the perceived live cell density in the live/dead stained fluorescence micrographs. This enhanced cell number could be due to the adhesive properties of PDA that have been shown to preferentially binds cells and promote proliferation.[28]

To determine the feasibility of non-invasively imaging and monitoring labeled scaffolds in a living animal, an in vivo study was conducted on a series of scaffolds. Labeled and unlabeled collagen hydrogels were formed in situ by subcutaneous injection in female Sprague Dawley rats. The scaffolds were monitored longitudinally on MRI up to 22 days post-implantation, and all animals were sacrificed for gross dissection (**Figures 7**).

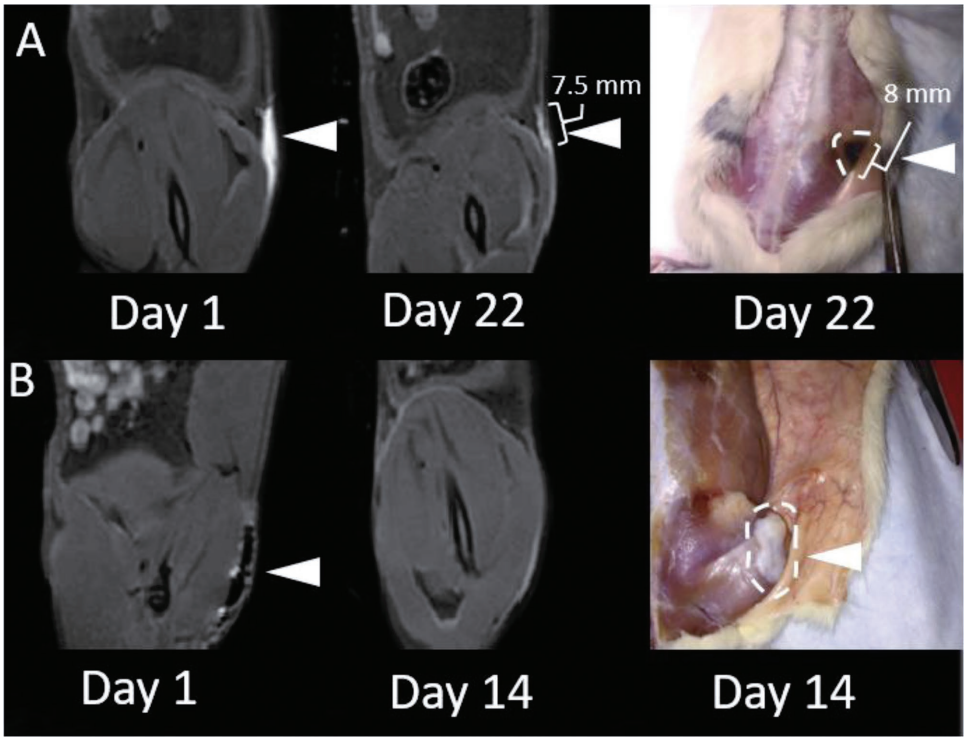

Figure 7. In vivo MRI monitoring of scaffold degradation. Fat-saturated T_1-weighted spin echo images over time and gross dissection of rats injected with A) 3 mg mL^{-1} collagen gel labeled with 0.2 mM $MnPNH_2$ and 0.25 mM PDA, and B) 10 mg mL^{-1} collagen gel unlabeled. MRI accurately delineated graft dimensions, as confirmed post-mortem on gross pathology on Day 22. Unlabeled gels were visible on MR on Day 1 but not on Day 14, when post-mortem confirmed the gel was still present.

$MnPNH_2$-PDA scaffolds could be accurately tracked and visualized for the full 22-day period using T_1-weighted MRI. The labeled scaffolds degraded over time, which was evident by a significant reduction in scaffold size, visualized by MRI and confirmed on gross pathology. Furthermore, a decrease in signal contrast from the interior of the scaffold was observed over the study period. This loss in signal and change in size can be attributed to bulk and surface degradation, respectively, indicating that as the scaffold degraded, the $MnPNH_2$ contrast agent was flushed away, resulting in signal loss. Gross dissection confirmed the accuracy of MRI in spatially delineating graft size and geometry even at 22 days (Figure 7A). In contrast, unlabeled collagen gels were not visible on MRI, except on Day 1 due to initial high water content (Figure 7B). Similarly distinct hyperintensity from labeled collagen scaffolds was observed in all animals, demonstrating the robustness of our labeling approach for in vivo monitoring and assessment of biomaterial scaffolds.

3. Conclusion

This work demonstrates a promising proof-of-principle method for creating biocompatible collagen scaffolds that are "trackable" on MRI. Multiple methods, including both passive and active binding, were investigated to label collagen scaffolds with a positive contrast-generating agent $MnPNH_2$. The active binding methods based on a PDA adhesive resulted in the highest contrast retention and signal enhancement. Labeled collagen scaffolds were visualized with excellent sensitivity both in vitro and in vivo. The superb sensitivity even permitted monitoring until nearly complete scaffold degradation in vivo, thus creating the potential for in vivo longitudinal monitoring of degradation rates. Although collagen was chosen as the prototype scaffold, our approach can, in principle, be readily extended to a variety of biomaterials. The proposed simple yet effective technique for scaffold labeling and monitoring lays the foundation for future investigations of biomaterial response in the body and for the creation of non-invasive, clinically oriented monitoring systems for patients.

4. Experimental Section

Materials: *N*,*N*-diisopropylethylamine (DIPEA), manganese chloride ($MnCl_2$), dimethylformamide (DMF), dimethyl sulfoxide (DMSO), concentrated sulfuric acid (H_2SO_4), 4-(2-hydroxyethyl)piperazine-1-ethanesulfonic acid (HEPES), Dulbecco's modified eagle's medium – high glucose (DMEM), sodium bicarbonate ($NaHCO_3$), hydrochloride (HCl), dopamine hydrochloride, collagenase from clostridium histolyticum (Type 1), ethtlenediaminetetraacetic acid (EDTA), phosphate buffered saline (PBS), Proliferation Reagent WST-1, and manganese standard for ICP were purchased from Sigma Aldrich (Steinheim, Germany). Nutragen (Bovine Collagen Solution, Type 1, 6 mg mL^{-1}), PureCol (Bovine Collagen Solution, Type 1, 3 mg mL^{-1}), and FibriCol (Bovine Collagen Solution, Type 1, 10 mg mL^{-1}) were purchased from Cedarlane Labs (Ontario, Canada). CyQuant Direct Cell Proliferation Assay C35011 was purchased from Thermo Fisher Scientific (MA, USA).

Calceinacetoxymethyl (Calcein AM) and ethidium homodimer-1 (EthD-1) were purchased from Invitrogen (CA, USA). Primary human umbilical vein endothelial cells, single donor, in EGM-2 from Lonza (Basel, Switzerland). VascuLife VEGF Endothelial Medium from Lifeline Cell Technologies (MD, USA). Pretreated regenerated cellulose dialysis tubing (MWCO: 1 kD) was purchased from Spectrum Labs (OH, USA). Ion-exchange resin (amberlite IR120, H form) was purchased from ACROS Organics. 5-(4-Aminophenyl)-10,15,20-(triphenyl)porphyrin was purchased from PorphyChem (Dijon, France). All chemicals were of appropriate analytical grade and were used without further purification.

Synthesis of $MnPNH_2$: Manganese 5-(4-aminophenyl)-10,15,20-(tri-4-sulfonatophenyl)porphyrin trisodium chloride ($MnPNH_2$) was synthesized following a modified protocol in literature for analogous porphyrin compounds.[35] In brief, the precursor 5-(4-aminophenyl)-10,15,20-(triphenyl)porphyrin (PorphyChem, France) was sulfonated with concentrated sulfuric acid at 75 °C to form the intermediate 5-(4-aminophenyl)-10,15,20-(tri-4-sulfonatophenyl)porphyrin trisodium (Apo-PNH_2). The intermediate was then purified by centrifugation and dialysis with pretreated regenerated cellulose dialysis tubing (MWCO: 1 kD). After purification, the intermediate was metallated with $MnCl_2$ in DMF and DIPEA at 135 °C for 3 h under reflux to form $MnPNH_2$. The degree of metallation was tracked by peak shift via UV analysis. $MnPNH_2$ was then distilled down and purified by silica column chromatography, dialysis and ion-exchange with Amberlite IR120, H form ion exchange resin. $MnPNH_2$ was then dried by lyophilization with a VirTis BenchTop Freeze Drier.

Characterization of Apo-PNH_2 and $MnPNH_2$: Apo-PNH_2 and $MnPNH_2$ identity and purity was determined by UV–visible spectra, ^{1}H NMR, HPLC, FAAS, and mass spectroscopy. UV–visible spectra were recorded on an Agilent 8453 UV–visible spectroscopy system. Absorption spectra of Apo-PNH_2 and $MnPNH_2$ were measured in HEPES buffer at 25 °C, λ_{max} = 415 nm and λ_{max} = 469 nm, ε = 93 552 $M^{-1}cm^{-1}$, respectively (Figure S2, Supporting Information). ^{1}H NMR spectra were recorded on a Bruker US 500 MHz system (Figure S1, Supporting Information). HPLC spectra were recorded using a PerkinElmer Series 200 system with UV/Vis detectors recording at 469 nm and using an acetonitrile and 10 mM ammonium acetate (NH_4OAc) gradient mix. Elution occurred at 2.20 min with 99.86% purity (Figure S3, Supporting Information). A Supelco Supercosil LC-18 column with dimensions 25 cm × 4.6 mm and 5 um beads was used. FAAS were recorded on a PerkinElmer AAnalyst 100 system with a Manganese Lumina Hollow Cathode Lamp. The Mn concentration determined by UV was compared to Mn concentration determined by FAAS to confirm that all excess Mn was removed. Mass spectroscopy was conducted on $MnPNH_2$ with an Agilent 6538 Q-TOF system in ESI MS Negative mode. ESI MS found m/z = 459.5138 [M^+], calculated for $C_{44}H_{26}MnN_5O_9S_3^{-2}$, m/z = 459.5142 (Figure S4, Supporting Information).

Synthesis of $MnPNH_2$ Labeled Collagen Scaffolds: Acid purified bovine type 1 collagen (Cedarlane, Canada) at concentrations 3, 6, or 10 mg mL^{-1} were mixed with DMEM (containing glucose and phenol red) and neutralized with sodium bicarbonate at 4 °C. This solution was then mixed either with $MnPNH_2$ only or $MnPNH_2$ and dopamine hydrochloride at different time points (0 or 24 h) and concentrations ($MnPNH_2$: 0, 0.1, 0.2 or 0.4 mM and dopamine hydrochloride: 0, 0.25, 0.5, or 2.5 mM). The solutions were then kept stirring at 4 °C for an additional 24 h. Afterward, the solutions were cross-linked to form gels by warming them up to room temperature for 1 h and then heating at physiological temperature 37 °C for 12 h. To remove any unbound chemicals, all scaffolds were then washed for 3 days in phosphate buffered saline at physiological pH. The buffer was exchanged every 3 h. Day 1 and day 3 of washing occurred at room temperature, while day 2 was conducted at the physiological temperature of 37 °C. After washing, gels were incubated in DMEMx1 for one day before any characterization or experimental studies.

Scanning Electron Microscopy (SEM): To assess changes in fiber morphology and density, scaffolds were flash frozen with liquid nitrogen and then freeze dried with a VirTis BenchTop Freeze Drier. The specimens were then sputter-coated with platinum and imaged using an environmental field emission SEM (Quanta FEG 250 ESEM, FEI Company, OR, USA) at 10 kV in a high-vacuum environment.

Magnetic Resonance Imaging (MRI): For in vitro MRI measurements, scaffolds were loaded into polystyrene phantoms and immersed in either DMEMx1 or PBSx1 at physiological pH and salt concentrations. MR relaxometry of the scaffolds was performed on a clinical 3.0-Tesla whole-body MR scanner (Achieva 3.0T TX, Philips Medical Systems, Best, the Netherlands) using a 32-channel transmit/receive head coil. High-resolution T_1-weighted images were acquired using a 2D spin-echo (SE) sequence: repetition time (TR) = 100 ms, echo time (TE) = 14.1 ms, 120 mm field-of-view (FOV), 3 mm slice thickness, 0.5 mm × 0.5 mm in-plane resolution, and number of signal averages (NSA) = 8. High-resolution T_2-weighted images were acquired using a 2D turbo spin-echo sequence: TR = 3000 ms, TE = 80 ms, NSA = 2, echo train length = 8.

Quantitative T_1 relaxation times were measured using a 2D inversion-recovery TSE sequence: inversion times (TI) = [50, 100, 250, 500, 750, 1000, 1250, 1500, 2000, 2500] ms, TR = 3000 ms, TE = 18.5 ms, TSE factor = 4, and the same voxel resolution as above. Quantitative T_2 relaxation times were measured using a multi-echo SE sequence: 32 echoes with TE spacing = 7.63 ms, TR = 2000 ms.

MRI data were transferred to an independent workstation for quantitative data analysis using in-house software developed in Matlab (v.8.3) (MathWorks, Natick, MA). Calculations of T_1 and T_2 times were performed on a pixel-by-pixel basis in each scaffold as described previously.[36,37] Relaxation times were then averaged over all pixels in each scaffold and reported as mean values and standard deviations.

Collagenase Assay and Characterization: Collagen scaffolds with and without $MnPNH_2$ and dopamine hydrochloride were prepared as before and immersed in PBSx1 (pH 7.4) with calcium and magnesium. Varying concentrations (4, 8, and 16 U mL^{-1}) of collagenase from clostridium histolyticum, Type 1 (Steinheim, Germany) were added to the scaffolds to induce enzymatic degradation. The scaffolds were incubated in these mixtures for 4 h at 37 °C. Afterward, enzymatic activity was quenched via the addition of 1 mL of 0.01 M EDTA. The scaffolds were then washed three times with 10× excess volume of PBSx1. The scaffolds were imaged by MRI using the sequences and analysis techniques described above. UV–vis analysis was carried out on the residual degradation solutions to determine the release profile of $MnPNH_2$ from the degraded scaffolds (Figure S5, Supporting Information). Scaffolds were prepared and assayed over three individual trials (n = 3).

Contraction Assay and Characterization: Collagen scaffolds with $MnPNH_2$ and dopamine hydrochloride were prepared as before but were solidified in triangular molds to aid with the identification of change in shape that may be due to degradation versus contraction. The gels were then immersed in PBSx1 (pH 7.4) without calcium and magnesium before contraction in a solution of 0.1 M HCl. The scaffolds were incubated in this mixture for 4 h at 37 °C. Afterward, the scaffolds were then washed three times with 10× excess volume of PBSx1. The scaffolds were imaged by MRI using the sequences and analysis techniques described above.

Cell Culture for Biocompatibility Analysis: For all biocompatibility assays, scaffolds were prepared as before and then seeded on top with primary human umbilical vein endothelial cells, single donor, in EGM-2 (Basel, Switzerland). The seeded cells were cultured in VascuLife VEGF Endothelial Medium (MD, USA). The DMSO control samples were cultured with medium containing 5% DMSO to provide a cell death positive control for all assays.

Live-Dead Staining and Microscopy: Scaffolds were prepared as stated before in 24 well plates. After gelation and washing, cells were seeded at a density of 40 000 cells per well and then cultured for 48 h. Prior to imaging, cells were incubated with 2 μM calceinacetoxymethyl (Calcein AM) live stain and 4 μM ethidium homodimer-1 (EthD-1) dead stain in PBSx1 with calcium and magnesium for 45 min at 37 °C. Stained cells were then imaged by fluorescence microscopy with a Leica DMi8 inverted epifluorescence microscope using a GFP filter cube to visualize the live stain and a TXR filter cube to visualize the dead stain.

Live Cell DNA Proliferation and Cytotoxicity Assay: Scaffolds were prepared as stated before in 96 well plates. After gelation and washing, cells were seeded at a density of 4000 cells per well and then cultured for 48 h. CyQuant Direct Nucleic acid stain and background suppressor stain (1:5 ratio) were then prepared in cell culture medium and added to each well. The wells were then incubated for 2 h at 37 °C before fluorescence was measured with a FITC filter set on a PerkinElmer Envision 2104 Multilabel Plate Reader (MA, USA). The fluorescence intensity directly corresponded to live cell DNA content due to the cell permeable nucleic acid stain and the dead cell background suppressor stain. This ensures that this assay measures both cell proliferation and cytotoxicity. Scaffolds were prepared and assayed over six individual trials ($n = 6$).

Metabolic Activity Assay: Scaffolds were prepared as stated before in 96 well plates. After gelation and washing, cells were seeded at a density of 4000 cells per well and then cultured for 48 h. Culture medium was then removed from each well and replaced with fresh media containing WST-1 reagent at a 1:10 dilution. The wells were then incubated for 1 h at 37 °C, after which the WST-1 containing medium was removed, and its absorbance at 450 nm was measured by a PerkinElmer Envision 2104 Multilabel Plate Reader (MA, USA). Scaffolds were prepared and assayed in triplicate ($n = 3$).

In Vivo Evaluation: All animal experiments were approved by the institutional animal care committee (protocol #36 668), and all procedures were conducted in accordance with the National Council on Animal Care. Five Sprague Dawley rats (Charles River Laboratories International, Inc., Wilmington, MA, USA) were used in a pilot study to evaluate the safety and efficacy of the labeled scaffolds. All methods of labeling were tested, and both $MnPNH_2$ and dopamine solutions were used as controls. Rats were injected subcutaneously with various solutions of $MnPNH_2$ (0, 0.1, or 0.2 mM), dopamine hydrochloride (0, 0.25, or 0.5 mM), neutralized un-cross-linked chilled collagen solution (3, 6, and 10 mg mL^{-1}), and neutralized un-cross-linked chilled collagen solutions labeled with dopamine (0, 0.25, or 0.5 mM) and/or $MnPNH_2$ (0, 0.1, or 0.2 mM). This set of conditions was chosen to determine the safety of the different compounds and the ideal labeling procedure for the most efficacious in vivo visualization of collagen scaffolds. All injections were conducted subcutaneously on the dorsal side of the animal at the following injection sites: base of the neck, right and left front limbs, and right and left hind limbs while the rat was under anesthesia at 3% isoflurane. After injection, the animal was kept under anesthesia at 2% isoflurane for an additional hour to ensure the collagen solutions were given adequate time to thermally cross-link in vivo at an internal temperature of 37 °C.

At days 1, 2, 3, 5, 7, 9, 16, and 22 post-implantation, MRI of the implanted scaffolds was performed on the 3.0-Tesla scanner with a 16-channel receive-only wrist coil. Rats were anethesized on 3% isofluane (with 2 L min^{-1} flow rate of 100% O2 at 50 psi). Once anesthetized, rats were transferred to the receiving coil and maintained on 2% isoflurane. Rats were placed prone, head first into the scanner and kept warm on a water-blanket heated by Heat Therapy Pump (HTP-1500, Andriotmedical) set at 41 °C. To visualize anatomic details, sagittal high-resolution T_1-weighted and T_2-weighted spin echo images were acquired. T_1-weighted images were acquired using a 2D SE sequence with fat suppression: TR = 2173 ms, TE = 13.6 ms, FOV = 130 mm, slice thickness = 3 mm, in-plane resolution is 0.6 mm × 0.6 mm, and NSA = 3. T_2-weighted images were acquired using a 2D turbo SE sequence: TR = 4000 ms, TE = 75 ms, NSA = 2, and similar resolutions as for T_1-weighted imaging.

Animals were sacrificed after 16 days for the animal bearing only control injections and after 22 days for all other animals. An incision was made to expose the collagen implants, which were then photographed and excised for gross analysis. The dimensions of the explants were noted.

Statistical Analysis: A two-way ANOVA was used to determine significant changes in the T_1 and T_2 relaxation times, with the variables being either the method of labeling and $MnPNH_2$ concentrations or the dose of dopamine and $MnPNH_2$ concentrations. For the degradation study, a one-way ANOVA was used to determine significant changes in UV absorbance, scaffold volume, or T_1/T_2 relaxation times as a function of collagenase concentration. A Tukey–Kramer test was used for post-hoc analysis. Significance is reported at a p-value of 5%.

Supporting Information

Supporting Information is available from the Wiley Online Library or from the author.

Acknowledgements

Natural Sciences and Engineering Research Council of Canada (#355795), Translational Biology and Engineering Program Seed Grant, IBBME Director's Kickstart Award, Canada First Research Excellence Fund Medicine by Design Team Project, Canada Foundation for Innovation/Ontario Research Fund (#34038), Ontario Graduate Scholarships.

Conflict of Interest

The authors declare no conflict of interest.

Keywords

biomaterial, biomedical engineering, magnetic resonance imaging, scaffold monitoring, tissue engineering

Received: August 28, 2018
Revised: November 29, 2018
Published online:

[1] L. Cen, K. G. Neoh, J. Sun, F. Hu, W. Liu, L. Cui, Y. Cao, *Adv. Funct. Mater.* **2009**, *19*, 1158.
[2] G. N. Nelson, J. D. Roh, T. L. Mirensky, Y. Wang, T. Yi, G. Tellides, J. S. Pober, P. Shkarin, E. M. Shapiro, W. M. Saltzman, X. Papademetris, T. M. Fahmy, C. K. Breuer, *FASEB J.* **2008**, *22*, 3888.
[3] Y. Liang, A. Bar-Shir, X. Song, A. A. Gilad, P. Walczak, J. W. Bulte, *Biomaterials* **2015**, *42*, 144.
[4] M. E. Mertens, A. Hermann, A. Buhren, L. Olde-Damink, D. Mockel, F. Gremse, J. Ehling, F. Kiessling, T. Lammers, *Adv. Funct. Mater.* **2014**, *24*, 754.
[5] J. Liu, K. Wang, J. Luan, Z. Wen, L. Wang, Z. Liu, G. Wu, R. Zhuo, *J. Mater. Chem. B* **2016**, *4*, 1343.
[6] W. Cheng, T. Ganesh, F. Martinez, J. Lam, H. Yoon, R. B. Macgregor, Jr ., T. J. Scholl, H. L. Cheng, X. A. Zhang, *J. Biol. Inorg. Chem.* **2014**, *19*, 229.
[7] M. E. Lynge, R. van der Westen, A. Postma, B. Stadler, *Nanoscale* **2011**, *3*, 4916.
[8] S. Hong, K. Y. Kim, H. J. Wook, S. Y. Park, K. D. Lee, D. Y. Lee, H. Lee, *Nanomedicine* **2011**, *6*, 793.
[9] P. Chen, J. Bornhorst, M. Aschner, *Front. Biosci.* **2018**, *23*, 1655.
[10] C. D. Davis, J. L. Greger, *Am. J. Clin. Nutr.* **1992**, *55*, 747.
[11] "Toxicological Profile for Manganese", Agency for Toxic Substances and Disease Registry, U.S. Department of Health and Human Services, **2012**.
[12] "FDA Drug Safety Communication: FDA evaluating the risk of brain deposits with repeated use of gadolinium-based contrast agents for

magnetic resonance imaging (MRI)", U.S. Food & Drug Administration, U.S. Department of Health and Human Services, July 27 **2015**.
[13] T. Kanda, T. Fukusato, M. Matsuda, K. Toyoda, H. Oba, J. Kotoku, T. Haruyama, K. Kitajima, S. Furui, *Radiology* **2015**, *276*, 228.
[14] S. Swaminathan, W. A. High, J. Ranville, T. D. Horn, K. Hiatt, M. Thomas, H. H. Brown, S. V. Shah, *Kidney Int.* **2008**, *73*, 1413.
[15] G. T. Hermanson, "Bioconjugate Techniques", 3rd edition, Academic Press, Boston **2013**, p. 1200.
[16] J. T. Nofiele, I. E. Haedicke, K. Zhu Yle, X. A. Zhang, H. L. Cheng, *J. Magn. Reson. Imaging* **2015**, *41*, 397.
[17] W. Cheng, *Ph.D. Thesis*, Unversity of Toronto, Toronto **2015**.
[18] Y. H. Ding, M. Floren, W. Tan, *Biosurf. Biotribol.* **2016**, *2*, 121.
[19] C. Y. Liu, C. J. Huang, *Langmuir* **2016**, *32*, 5019.
[20] R. Parenteau-Bareil, R. Gauvin, F. Berthod, *Materials* **2010**, *3*, 1863.
[21] F. G. Lyons, A. A. Al-Munajjed, S. M. Kieran, M. E. Toner, C. M. Murphy, G. P. Duffy, F. J. O'Brien, *Biomaterials* **2010**, *31*, 9232.
[22] G. T. Kose, F. Korkusuz, A. Ozkul, Y. Soysal, T. Ozdemir, C. Yildiz, V. Hasirci, *Biomaterials* **2005**, *26*, 5187.
[23] J. Glowacki, S. Mizuno, *Biopolymers* **2008**, *89*, 338.
[24] Q. Lu, K. Ganesan, D. T. Simionescu, N. R. Vyavahare, *Biomaterials* **2004**, *25*, 5227.
[25] L. E. Freed, G. Vunjak-Novakovic, R. J. Biron, D. B. Eagles, D. C. Lesnoy, S. K. Barlow, R. Langer, *Biotechnology* **1994**, *12*, 689.
[26] T. R. Chan, P. J. Stahl, S. M. Yu, *Adv. Funct. Mater.* **2011**, *21*, 4252.
[27] H. Lee, S. M. Dellatore, W. M. Miller, P. B. Messersmith, *Science* **2007**, *318*, 426.
[28] S. Zhu, Z. Gu, S. Xiong, Y. An, Y. Liu, T. Yin, J. You, Y. Hu, *RSC Adv.* **2016**, *6*, 66180.
[29] Z. G. Liu, S. X. Qu, J. Weng, *Prog. Chem.* **2015**, *27*, 212.
[30] S. M. Kang, N. S. Hwang, J. Yeom, S. Y. Park, P. B. Messersmith, I. S. Choi, R. Langer, D. G. Anderson, H. Lee, *Adv. Funct. Mater.* **2012**, *22*, 2949.
[31] H. L. Cheng, I. E. Haedicke, W. Cheng, J. T. Nofiele, X. A. Zhang, *J. Mag. Reson. Imaging* **2014**, *40*, 1474.
[32] J. Z. Bojorquez, S. Bricq, C. Acquitter, F. Brunotte, P. M. Walker, A. Lalande, *Magn. Reson. Imaging* **2017**, *35*, 69.
[33] A. P. McGuigan, M. V. Sefton, *Proc. Natl. Acad. Sci. U.S.A.* **2006**, *103*, 11461.
[34] O. F. Khan, M. V. Sefton, *Trends Biotechnol.* **2011**, *29*, 379.
[35] J. S. Lindsey, S. Prathapan, T. E. Johnson, R. W. Wagner, *Tetrahedron* **1994**, *50*, 8941.
[36] H. L. Cheng, G. A. Wright, *Magn. Reson. Imaging* **2006**, *55*, 566.
[37] M. Beaumont, I. Odame, P. S. Babyn, L. Vidarsson, M. Kirby-Allen, H. L. Cheng, *J. Mag. Reson. Imaging* **2009**, *30*, 313.